Dielectric function in HgTe between 8 and 300 °K

M. Grynberg,* R. Le Toullec, and M. Balkanski
Laboratoire de Physique des Solides, de l'Université de Paris VI, Laboratoire associe au Centre National de la Recherche Scientifique, II, quai Saint-Bernard, Paris V, France
(Received 6 March 1972)

Reflectivity spectra of HgTe were measured in the spectral region from 80 to 600 cm^{-1} at temperatures between 8 and 300 °K. The wave numbers of the transverse-optical phonon $\omega_{TO} = 117$ cm^{-1} and longitudinal-optical phonon $\omega_{LO} = 132$ cm^{-1} at 8 °K were determined. The total dielectric function including the interband Γ_8-Γ_8 contribution was analyzed. Plasmon-phonon dispersion diagrams were obtained. The theoretical analysis is compared with experimental results at all temperatures. Possible consequences of the adiabatic approximation breaking down in zero-gap semiconductors is examined. A new low-frequency mode is reported, its temperature dependence is given, and its origin is discussed from physicochemical arguments.

I. INTRODUCTION

Small-gap or zero-gap semiconductors have recently attracted considerable attention as regards their galvanomagnetic and photoelectronic properties. This class of materials gives one an opportunity of studying solid phenomena in a domain where the energies of electronic interband transitions and lattice vibrations are comparable. Apart from this, the obvious potentialities for applications undoubtedly have done much to spur the study of those crystals. Nevertheless, comparatively little is known about the medium and far-infrared optical constants of those materials, especially in the region of fundamental lattice vibrations (LO and TO phonons).

This is true for the IV-VI class, lead and tin chalcogenides with a NaCl crystal structure, and also for the II-VI class with a zinc-blende structure. Mercury telluride, whose band structure is shown in Fig. 1, is an example of this class of materials.

The earliest work on the phonon spectrum of HgTe was that of Dickey and Mavroides[1] at 8 °K, then that of Ivanov-Omskii, Kolomiets, Molkova, Markovand, and Mechtiev at 80 °K.[2] The observation of infrared-active phonon modes is complicated by the band structure of HgTe. In the region of the LO and TO modes, around 100 wave numbers, at nonzero temperatures, electronic intraband transitions and interband Γ_8-Γ_8 transitions should overlap with the infrared-active TO mode. We shall see moreover that this is an oversimplified view of the problem and that other oscillators have to be taken into account to derive the right parameters for lattice vibrations and distinguish quantitatively among several contributions to the dielectric function.

In this paper, we first give an analysis of different contributions to the real and imaginary parts of the dielectric function and present experimental results of reflectivity in HgTe between 8 and 300 °K. These results are compared with theory and then we discuss the behavior of the different oscillators and the limits of validity of our interpretation.

II. THEORY

The experimental results presented in this paper clearly show that in the infrared spectral region several oscillators have to be considered in order to explain the shape of the optical spectra. Because HgTe is cubic with two different atoms per unit cell, it has one infrared-active fundamental phonon mode at the center of the zone. Moreover, at high temperatures, infrared dispersion on free carries, mostly electrons, is clearly present.

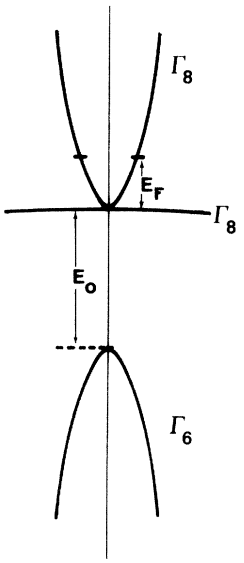

FIG. 1. Schematic band structure of HgTe at the center of the Brillouin zone. Off-Γ overlaps of the Γ_8 bands due to linear terms in $\vec{k}$ are neglected.

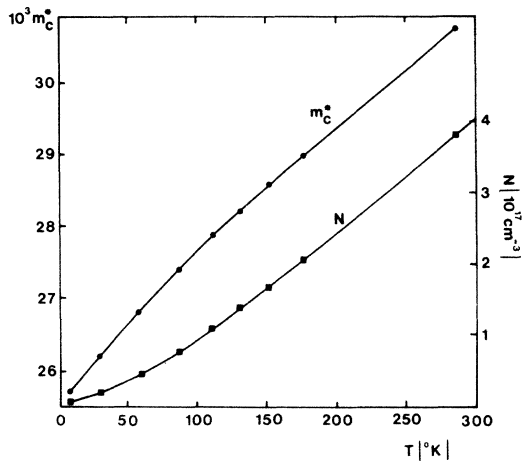

FIG. 2. Temperature variation of effective mass ratio $m_c^* = m_c/m_0$ at the Fermi level, calculated for samples with 6×10^{15} cm^{-3} n-type extrinsic carriers (left-hand scale of ordinates). Temperature variation of electron concentration N for the same samples (right-hand scale of ordinates).

The general form of the complex dielectric function can be written

$$\epsilon(\omega) = \epsilon_\infty + \Delta\epsilon_{\text{inter}} + \Delta\epsilon_{\text{intra}} + \Delta\epsilon_{\text{ph}}\ , \tag{1}$$

where ϵ_∞ is the high-frequency dielectric constant due to all interband transitions except $\Gamma_8 \rightarrow \Gamma_8$, $\Delta\epsilon_{\text{inter}}$ is the contribution due to $\Gamma_8 \rightarrow \Gamma_8$ interband transitions, $\Delta\epsilon_{\text{intra}}$ is the contribution due to intraband carriers in the Γ_8 band, $\Delta\epsilon_{\text{ph}}$ is the contribution due to phonons, and Ω is the wave number of light with angular frequency $\omega = 2\pi c\Omega$.

A. Interband contribution: $\Delta\epsilon_{\text{inter}}$

A consequence of the zero value for the gap at the Γ point is that interband $\Gamma_8 \rightarrow \Gamma_8$ transitions from the heavy-hole valence band to the electron conduction band, although symmetry forbidden to first order, are nonetheless possible for all photon energies in intrinsic material. The influence of such transitions on the static dielectric function of zero-gap semiconductors was studied by several authors.[3–6] Comparatively little has been done on the interband contribution to the dynamic dielectric function $\Delta\epsilon_{\text{inter}}(\omega)$. Sherrington and Kohn calculated the frequency-dependent dielectric function for α-Sn[7] at 0 °K and, recently, Broerman[8] gave expressions for the dielectric function of α-Sn in the infrared at finite but very low temperatures.

Let us first derive the relevant expression for $\Delta\epsilon_{\text{inter}}$. The following conditions are used here: The optical $\Gamma_8 \rightarrow \Gamma_8$ transition is direct ($\vec{k}$ selection rule). The matrix element is linear in $|\vec{k}|$. The material contains a negligible concentration of extrinsic charge carriers at sufficiently high temperatures. Since the hole effective mass m_v is much larger than m_c, we take it as infinite as regards the density of states. Nonparabolicity of the band is taken into account to calculate $m_c^*(E)$ and E_F (Fermi level) of electrons relative to the bottom of the band (Fig. 2) as a function of temperature. At a given temperature, the effective mass is taken as constant and equal to its value at the Fermi level $m_c^*(E_F)$: This curve was calculated taking into account Kane-type nonparabolicity of the Γ_8 conduction band and linear variation of the $\Gamma_6 \rightarrow \Gamma_8$ interaction gap with temperature (300 and 160 meV at 4 and 300 °K, respectively).

At finite temperature, taking into account the occupancy of the initial and final states, in the random-phase-approximation (RPA) formalism, the contribution of transitions between valence and conduction bands to the imaginary part of the dielectric function is given by

$$\Delta\epsilon''_{\text{inter},k,v,c}(\omega,T) = \frac{\hbar^2 4\pi^2 e^2}{m_0^2}\ \frac{|\langle \vec{k}, c|p|\vec{k}, v\rangle|^2}{|E_c(\vec{k}) - E_v(\vec{k})|^2} \times\{\delta[\hbar\omega - E_c(\vec{k}) + E_v(\vec{k})]f_v(1-f_c) - \delta[-\hbar\omega + E_c(\vec{k}) - E_v(\vec{k})]f_c(1-f_v)\}\ , \tag{2}$$

with

$$f_v = (1+e^{-E_F/kT})^{-1}\ , \qquad f_c = (1+e^{(E_c-E_F)/kT})^{-1}\ . \tag{3}$$

Here, m_0 is the free-electron mass, $|\vec{k}, v\rangle$ and $|\vec{k}, c\rangle$ denote valence- and conduction-band states, p is the projection of the momentum operator on the direction of incident light, and E is the energy of the states with the origin at the Γ_8 point. The transition probability

$$|\langle \vec{k}, c|p|\vec{k}, v\rangle|^2 = \tfrac{3}{16}\hbar^2 k^2 (m_0^2/\mu^2)\sin^2\theta\ , \tag{4}$$

where $\mu^{-1} = m_c^{-1} + m_v^{-1}$ and θ is the angle between $\vec{k}$ and $\vec{q}$, has been calculated by Sherrington and Kohn.[7] Setting

$$A = (2m_c)^{1/2} e^2/\hbar\ , \tag{5}$$

we get

$$\Delta\epsilon''_{\text{inter}}(\omega,T) = A(\hbar\omega)^{-1/2}[(1+e^{-E_F/kT})^{-1}(1+e^{(E_F-\hbar\omega)/kT})^{-1} - (1+e^{E_F/kT})^{-1}(1+e^{(-E_F+\hbar\omega)/kT})^{-1}]\ . \tag{6}$$

The calculated curves of $\Delta\epsilon''(\omega)$ for different temperatures are shown in Fig. 3. In these calculations we have used effective masses on the Fermi levels and electron concentrations obtained by Hall-effect measurements as shown in Fig. 2.

The real part of $\Delta\epsilon'_{\text{inter}}$ is obtained by performing the Kramers-Krönig inversion on the expression of $\Delta\epsilon''_{\text{inter}}$, which amounts to solving

$\Delta\epsilon'_{\text{inter}}(\omega)$

$$= \frac{2A}{\pi}\left(\frac{1}{1+e^{-E_F/kT}}\int_0^\infty \frac{\omega'^{1/2}d\omega'}{(\omega'^2-\omega^2)(1+e^{(E_F-\hbar\omega')/kT})}\right.$$

$$\left. - \frac{1}{1+e^{E_F/kT}}\int_0^\infty \frac{\omega'^{1/2}d\omega'}{(\omega'^2-\omega^2)(1+e^{(-E_F+\hbar\omega')/kT})}\right) . \quad (7)$$

The integration was performed by the method of residues

$$\Delta\epsilon'_{\text{inter}} = A\left(\frac{1}{(\hbar\omega)^{1/2}}\left[(1+e^{-E_F/\beta})^{-1}(1+e^{(E_F+\hbar\omega)/\beta})^{-1}\right.\right.$$

$$\left. - (1+e^{E_F/\beta})^{-1}(1+e^{(-E_F-\hbar\omega)/\beta})^{-1}\right]$$

$$\left. + \sum_{\nu=0}^{\infty} \frac{4\beta(E_F^2+P_\nu^2)^{1/4}\sin(\theta_\nu - \frac{1}{2}\Phi_\nu)}{[(E_F^2+\hbar^2\omega^2-P_\nu^2)^2+4E_F^2P_\nu^2]^{1/2}}\right), \quad (8)$$

with

$$\beta = kT\ , \quad P_\nu = \pi\beta(2\nu+1)\ ,$$

$$\tan\theta_\nu = \frac{2E_FP_\nu}{E_F^2+\hbar^2\omega^2-P_\nu^2}\ , \quad \tan\Phi_\nu = \frac{P_\nu}{E_F}\ .$$

This series has rather slow convergence (like $\nu^{-3/2}$) However, in the case of the calculation of $\Delta\epsilon'(\omega)$ for different temperatures shown in Fig. 4, 1000 terms were sufficient.

B. Intraband contribution: $\Delta\epsilon_{\text{intra}}$

The free-carriers contribution according to the classical Drude-Zener theory is

$$\Delta\epsilon_{\text{intra}} = -\frac{Ne^2}{\pi c^2 m_c}\frac{1}{\Omega^2+i\Gamma\Omega}\ , \quad (9)$$

Γ is the damping parameter for free carriers (in cm^{-1}).

C. Phonon contribution: ΔE_{ph}

In the frame of the classical theory of independent harmonic oscillators, the phonon contribution to the dielectric function is given by

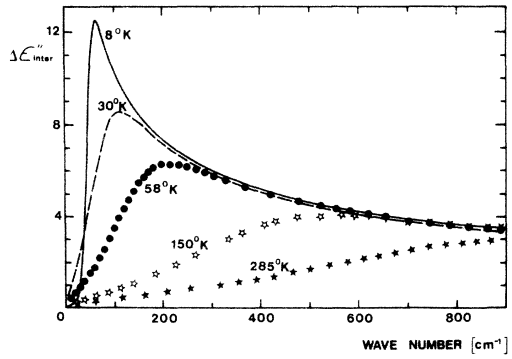

FIG. 3. Imaginary part $\Delta\epsilon''_{\text{inter}}$ of the Γ_8-Γ_8 interband contribution to dielectric function, vs wave number for several temperatures, calculated from Eq. (6).

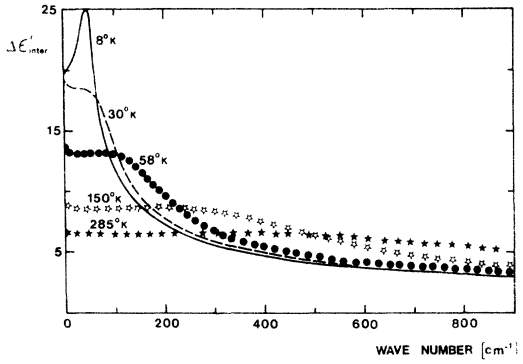

FIG. 4. Real part $\Delta\epsilon'_{\text{inter}}$ of the interband Γ_8-Γ_8 contribution to dielectric function vs wave number for several temperatures, calculated from Eq. (8).

$$\Delta\epsilon_{\text{ph}} = \sum_j \frac{F_j\Omega_j^2}{\Omega_j^2-\Omega^2-i\Gamma_j\Omega}\ , \quad (10)$$

where Ω_j is the wave number of the transverse mode for each oscillator in cm^{-1}, F_j the oscillator strengths, and Γ_j the damping parameters in cm^{-1}.

In the case we shall discuss here, two independent lattice oscillators ($j=2$) contribute to the dielectric function.

Equation (1) can then be written as a set of separate equations for the real and imaginary parts of the wave-number-dependent dielectric function:

$$\epsilon(\Omega) = \epsilon'(\Omega) + i\epsilon''(\Omega)\ ,$$

with

$$\epsilon' = \epsilon_\infty + \frac{F_1(\Omega_1^2-\Omega^2)\Omega_1^2}{(\Omega_1^2-\Omega^2)^2+\Gamma_1^2\Omega^2} + \frac{F_2(\Omega_2^2-\Omega^2)\Omega_2^2}{(\Omega_2^2-\Omega^2)^2+\Gamma_2^2\Omega^2}$$

$$- \frac{Ne^2}{\pi c^2 m_c(\Omega^2+\Gamma^2)} + \Delta\epsilon'_{\text{inter}}(\Omega)\ , \quad (11)$$

$$\epsilon'' = \frac{F_1\Gamma_1\Omega_1^2\Omega}{(\Omega_1^2-\Omega^2)^2+\Gamma_1^2\Omega^2} + \frac{F_2\Gamma_2\Omega_2^2\Omega}{(\Omega_2^2-\Omega^2)^2+\Gamma_2^2\Omega^2}$$

$$+ \frac{Ne^2\Gamma}{\pi c^2 m_c\Omega(\Omega^2+\Gamma^2)} + \Delta\epsilon''_{\text{inter}}(\Omega)\ . \quad (12)$$

III. EXPERIMENTS

A. Samples and experimental technique

Crystalline slabs of HgTe typically 60 μ in thickness were obtained from liquid-phase deposition by slow cooling of tellurium in a mercury bath. (The method of crystal preparation is described in the thesis work of Mycielski.[15]) Hall-effect measurements on these samples showed concentrations of n-type carriers of 4.2×10^{17} and 6.2×10^{16} cm^{-3} at 300 and 77 °K. At 4.2 °K, the samples still had $n\sim 6\times10^{15}$ cm^{-3} with a mobility of the order of 6×10^5 $\text{cm}^2\ \text{V}^{-1}\ \text{sec}^{-1}$. For galvanomagnetic measurements, samples were mechanically free except for gold wire electrodes attached to the surface

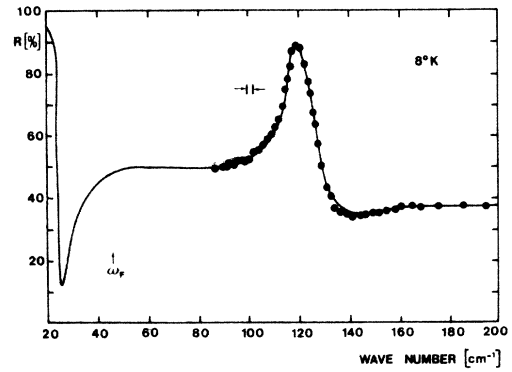

FIG. 5. Reflectivity curves vs wave number for 8 °K. Dots are experimental points. Solid curves are calculated by the method described in Sec. IV. The position of the Fermi level is shown as ω_F.

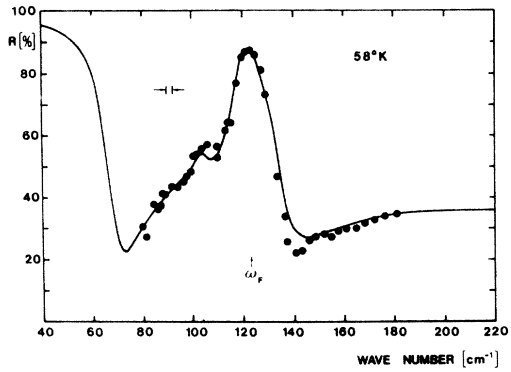

FIG. 7. Reflectivity curves vs wave number for 58 °K. Dots are experimental points. Solid curves are calculated by the method described in Sec. IV. The position of the Fermi level is shown as ω_F.

with silver paint, which proved to be good quality contacts. The samples are quasimonocrystalline layers in the (111) plane with a very small disorientation of the crystallites in the slab plane.

In the region of interest between 125 and 40 μ (80 to 250 wave numbers) the absorption coefficient was too high ($\alpha > 10^3$ cm^{-3}) to allow reliable transmission measurements, and the optical constants were derived from reflectivity measurements. These were performed in a vacuum grating spectrometer, conceived and built in the Laboratoire de Physique des Solides, with transmission and reflection filters. A Golay pneumatic cell with lock-in amplification was used.[9] The sample holder was in a low-temperature gas-exchange cell separated from the vacuum by crystal quartz, cesium iodide or Mylar windows. In this way, the temperature of the sample itself was quite accurately known since there was no problem of thermal contact with the cooling tip. The temperature of the cold finger and of the exchange gas was measured by a calibrated GaAs diode and monitored by a platinum-wire thermometer controlling an electrical heater. Temperature stability was achieved within ± 1 °K. Reflectivity from the HgTe surface was measured point by point relative to a metallic mirror at each wavelength in the region of interest. Stray light coming from the cold chamber windows was strongly reduced by mounting the sample at an angle with the windows plane (about 15°). Incidence of the sample was quasinormal (about 10°). Stray light reflected by the windows was measured and accounted for at each wavelength (about 5% of total reflection) for crystal windows and was negligible for Mylar windows. Over-all spectral resolution was $\Delta\nu = 3$ cm^{-1} in the region 80–160 cm^{-1} wave numbers, this value being limited by signal-to-noise ratio.

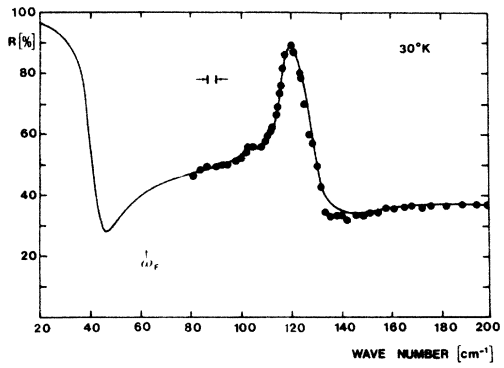

FIG. 6. Reflectivity curves vs wave number for 30 °K. Dots are experimental points. Solid curves are calculated by the method described in Sec. IV. The position of the Fermi level is shown as ω_F.

B. Experimental results

Absolute values for reflectivity vs wave number are given in Figs. 5–12. Other spectra at intermediate temperatures were measured and analyzed, but need not be shown here. In these figures, dots represent experimental points at one wavelength. The full line is a theoretical fit, the parameters of which are given below. The qualitative features of these spectra are readily apparent: the phonon-mode spectrum, which is isolated at 8 °K and then mixed in the plasma mode at higher temperatures, but is always visible in the region 100–130 cm^{-1}; the variation in frequency of the plasmon-phonon minima with increasing temperature, which are directly observable at 87 °K and above; at intermediate temperatures, a more complicated structure around 100 cm^{-1} due to the interaction of plasmon modes with two phononlike oscillators, as is discussed in Sec. VI.

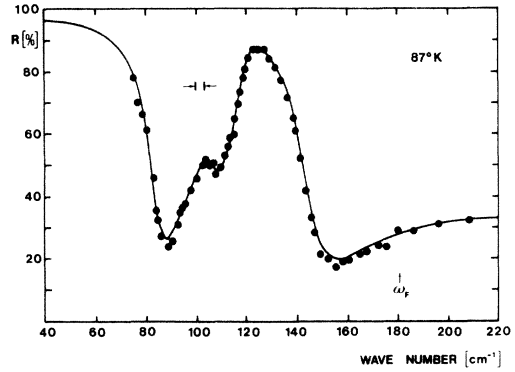

FIG. 8. Reflectivity curves vs wave number for 87 °K. Dots are experimental points. Solid curves are calculated by the method described in Sec. IV. The position of the Fermi level is shown as ω_F.

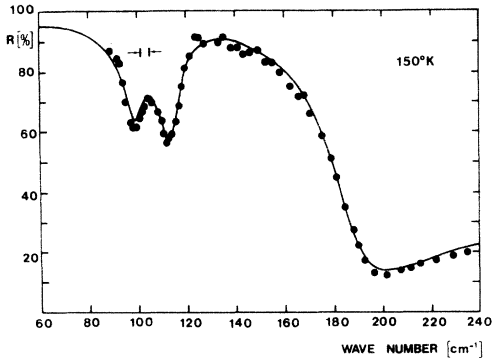

FIG. 10. Reflectivity curves vs wave number for 150 °K. Dots are experimental points. Solid curves are calculated by the method described in Sec. IV.

In Figs. 13 and 14, two typical results are presented for the values of $\mathrm{Im} - \epsilon^{-1} = \epsilon''/(\epsilon''^2 + \epsilon'^2)$ and ϵ'' derived from reflectivity curves at 8 and 110 °K by a Kramers-Krönig analysis. Measurements were made up to 600 cm^{-1} and the reflectivity on the high-frequency side was taken as flat above this wave number at all temperatures. On the low-frequency side, the reflectivity curves were extrapolated to a constant value. These extrapolations have no influence on the position of the peaks except at 30 and 58 °K. At these temperatures, a Kramers-Krönig inversion was not possible, since the low-frequency minimum was not observable, being beyond our spectral range (80 cm^{-1}) and still too close to be neglected for a Kramers-Krönig inversion.

Maxima of ϵ'' correspond to the frequency of transverse (dissipative) oscillators. The crystal TO frequency is thus visible as a strong peak in ϵ'' at $\Omega_1 = \omega_1/2\pi c = 117$ cm^{-1} at 8 °K (Fig. 13) and 118 cm^{-1} at 110 °K. The temperature variation of this TO frequency is plotted against temperature in Fig. 15. We may note that the result for Ω_1 is in good agreement at 8 °K with Raman scattering measurements.[10] A distinct maximum Ω_2 appears in ϵ'' at slightly smaller wave numbers. Its temperature dependence is given in Fig. 15. Points on the Ω_1 and Ω_2 frequency curve vs temperature (Fig. 15) at 30 and 58 °K, where a Kramers-Krönig inversion could not be performed, only represent the frequencies that had to be introduced into the reflectivity fit to account for the variation of reflectivity in this region.

Maxima of the $\epsilon''/(\epsilon''^2 + \epsilon'^2) = \mathrm{Im} - \epsilon^{-1}$ curve are connected with oscillators having longitudinal polarization character. At 8 °K, only the LO phonon mode is clearly apparent. At higher temperatures, e.g., 110 °K, two principal maxima correspond to Ω_+ and Ω_- plasmon-phonon coupled modes,[11,12] whereas the small maximum at ~ 107 cm^{-1} is connected with another mode Ω_2.

The parameters of these oscillators were evaluated in the following way: The background coming

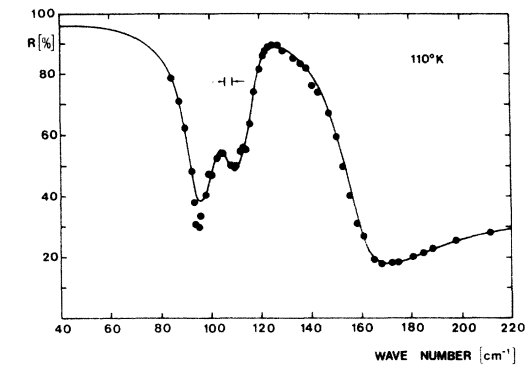

FIG. 9. Reflectivity curves vs wave number for 110 °K. Dots are experimental points. Solid curves are calculated by the method described in Sec. IV.

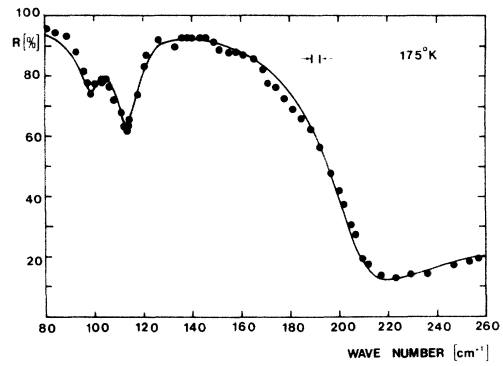

FIG. 11. Reflectivity curves vs wave number for 175 °K. Dots are experimental points. Solid curves are calculated by the method described in Sec. IV.

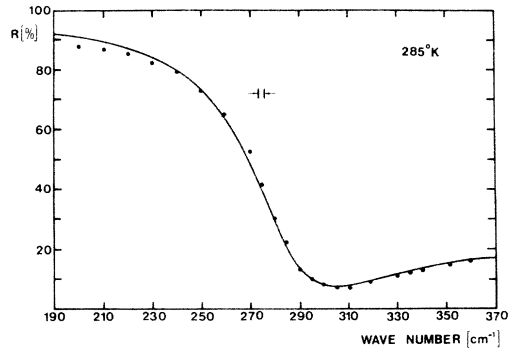

FIG. 12. Reflectivity curves vs wave number for 285 °K. Dots are experimental points. Solid curves are calculated by the method described in Sec. IV.

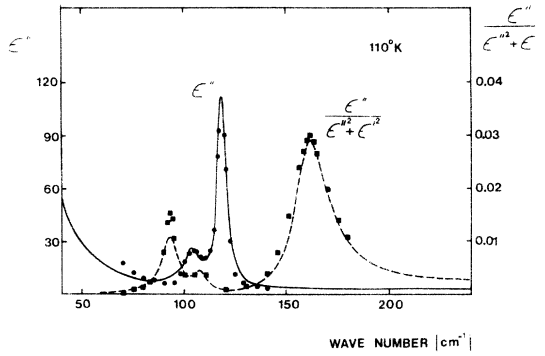

FIG. 14. Imaginary part ϵ'' of dielectric function (solid line) and $\mathrm{Im} - \epsilon^{-1} = \epsilon''/(\epsilon''^2 + \epsilon'^2)$ (dashed line) vs wave number at 110 °K. Curves were obtained from Eqs. (11) and (12). Solid points and squares were obtained from a Kramers-Krönig analysis of experimental reflectivity at 110 °K. Two transverse modes (corresponding to maxima in ϵ''), $\Omega_1 = \omega_{TO}$ and Ω_2, are present, as well as three longitudinal solutions [maxima of $\epsilon''/(\epsilon''^2 + \epsilon'^2)$].

from the interband and intraband contribution to ϵ'' was subtracted and the remaining peaks were decomposed into two Lorentzian curves. The temperature of the damping parameters Γ_1 and Γ_2 (half-width of the ϵ'' peaks associated with the Ω_1, TO phonon, and Ω_2 modes) is exhibited in Fig. 16. The oscillator strength is derived from the $\epsilon''(\omega)$ curves by the usual formula

$$F = \frac{2}{\pi} \int_{\text{peak}} \frac{\epsilon''(\omega)}{\omega}\, d\omega \,. \tag{13}$$

F_1, the oscillator strength of the fundamental TO phonon, is practically temperature independent: $F_1 = 4.7$. Conversely, F_2 is strongly temperature dependent and weaker in intensity. F_2 vs temperature is plotted in Fig. 17. The dielectric constant jump ($\simeq F_2$) due to this mode is larger than unity above 87 °K, which denotes a fairly strong oscillator. Finally, the experimental data that we used as a starting point for the calculations can be summarized by the following set of parameters: Ω_1 (TO mode) and Ω_2 vs temperature, as given in Fig. 15 for $87 < T < 285$ °K, $\Omega_1 = 117$ cm^{-1} at 8 °K; Γ_1 and Γ_2 vs temperature, as given in Fig. 16 in the same temperature regions; and $F_1 = 4.7$ and F_2 vs temperature for $87 < T < 285$ °K, as shown in Fig. 17.

All these parameters were evaluated from the experimental curves similar to those in Figs. 13 and 14.

One qualitative feature that should be pointed out is visible in Figs. 8–11: As the temperature increases, and N (number of electrons/cm^3) grows, the Ω_- solution for plasmon-phonon modes (near to the first reflectivity minimum just below 100 cm^{-1})

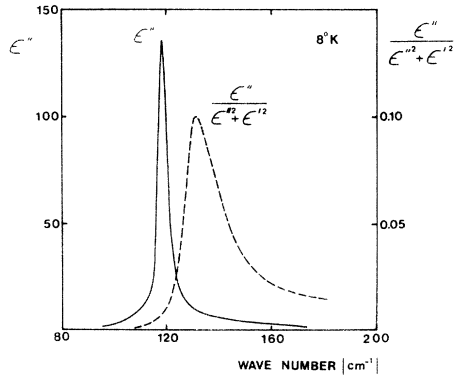

FIG. 13. Imaginary part ϵ'' of the dielectric function (solid line) and $\mathrm{Im} - \epsilon^{-1} = \epsilon''/(\epsilon''^2 + \epsilon'^2)$ (dashed curve) vs wave number at 8 °K, obtained by a Kramers-Krönig analysis of the experimental reflectivity curve. Maxima of ϵ'' and $\epsilon''/(\epsilon''^2 + \epsilon'^2)$ correspond to $\Omega_{TO} = 117$ cm^{-1} and $\Omega_{LO} = 132$ cm^{-1}, respectively.

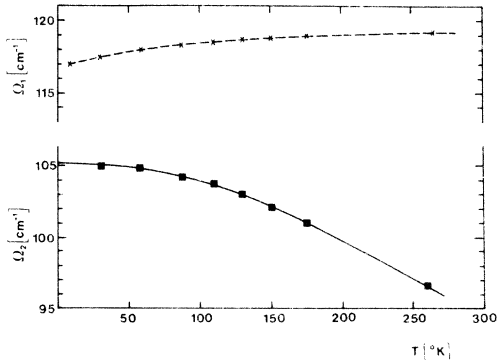

FIG. 15. Temperature dependence of Ω_1 and Ω_2 modes. Experimental values obtained from a Kramers-Krönig analysis of reflectivity data are marked as crosses (Ω_1) and solid squares (Ω_2). Curve of Ω_2 (T) was extrapolated in the temperature region below 30 °K.

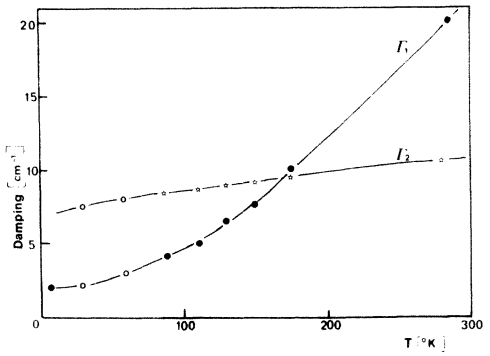

FIG. 16. Temperature dependence of damping parameters Γ_1 and Γ_2. Solid points and stars correspond to the half-width of $\epsilon''(\omega)$ for Ω_1 and Ω_2 (Kramers-Krönig analysis of reflectivity spectra). Open circles are the extrapolated values used in the theoretical fit.

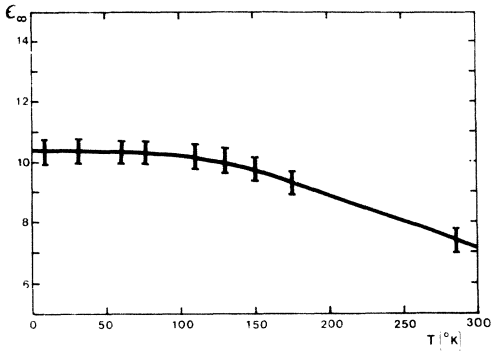

FIG. 18. Temperature dependence of ϵ_∞ as a parameter in Eqs. (11) and (12) to fit with experimental reflectivity.

comes closer and closer to the first reflectivity maximum (just above 100 cm^{-1}) representative of mode Ω_2 but does not pass it. This type of interaction with the free-carrier plasma suggests a transverse character for mode Ω_2.

IV. REFLECTIVITY FIT

Reflectivity was calculated from Eqs. (11) and (12) using the relations

$$\epsilon''(\omega) = 2n\kappa\,, \quad \epsilon'(\omega) = n^2 - \kappa^2\,, \tag{14}$$

and

$$R = [(n-1)^2 + \kappa^2]/[(n+1)^2 + \kappa^2]\,, \tag{15}$$

where n is the refractive index, κ the extinction coefficient, and R the reflectivity.

The temperature dependence of the parameters in these equations has been given in Fig. 2 for N and m_c, in Figs. 3 and 4 for $\Delta\epsilon''_{\text{inter}}$ and $\Delta\epsilon'_{\text{inter}}$, in Figs. 15–17 for Ω_1, Ω_2, Γ_1, Γ_2, and F_2. Only Γ and ϵ_∞ remain to be evaluated.

One should note that ϵ_∞ cannot be given directly by reflectivity curves for $\omega \gg \omega_{TO}$ as in the case of finite-gap semiconductors, where $E_g \gg \hbar\omega_{TO}$ and where direct plotting of the square of the refractive index vs λ^2 extrapolates to ϵ_∞. Here, the complicated variation of $\Delta\epsilon_{\text{inter}}$ makes it necessary to treat ϵ_∞ as a fitting parameter. The best fit for parameters ϵ_∞ and Γ was calculated by a computer procedure and the results for reflectivity are given as solid lines in Figs. 5–12. Corresponding values for ϵ_∞ and Γ as a function of temperatures are given in Figs. 18 and 19. An iterative procedure was then used to check the error margin of the parameters obtained from experiment, especially F_1, which could not be varied by more than $0.2(F_1 = 4.7 \pm 0.2)$, which is smaller than the experimental uncertainty of the area under the $\epsilon''(\omega)$

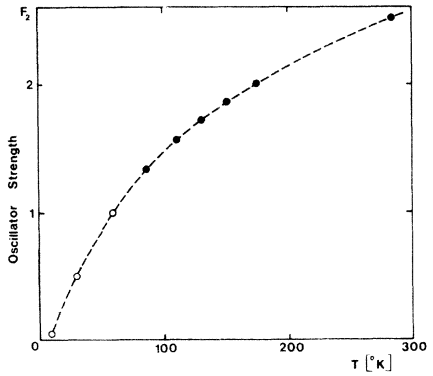

FIG. 17. Temperature dependence of oscillator strength F_2. Solid circles correspond to experimental values evaluated by Eq. (13) from a Kramers-Krönig analysis of reflectivity. Open circles correspond to extrapolated values used in the theoretical fit.

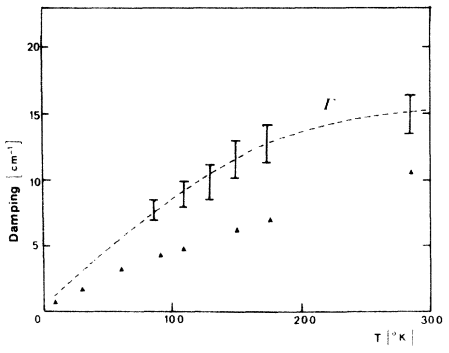

FIG. 19. Temperature variation of plasma-damping parameter Γ obtained as a parameter in Eqs. (11) and (12) to fit with experimental reflectivity. Solid triangles correspond to the static damping parameter [Eq. (16)] calculated from our galvanomagnetic measurements results and from Ref. 13. For temperatures below 87 °K, the dashed curve is our extrapolation.

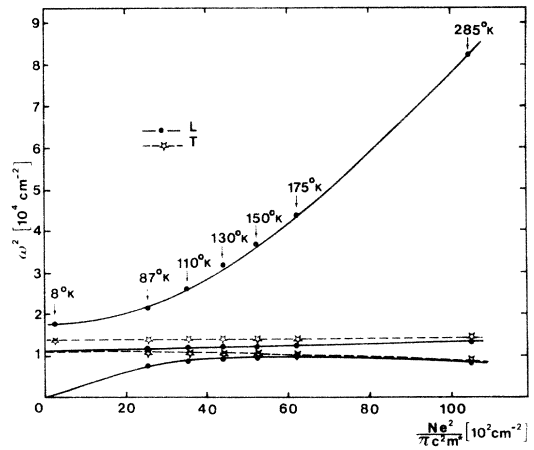

FIG. 20. Plasmon-phonon dispersion curve. Solid points and stars correspond to longitudinal and transverse modes, respectively [maxima of experimental $\epsilon''/(\epsilon''^2+\epsilon'^2)$ and ϵ'' (ω) curves, see Fig. 14]. Solid and dashed lines correspond to longitudinal and transverse solutions of Eqs. (11) and (12). Absolute temperature are indicated (arrows) for each experimental point.

curves. Variations of ϵ_∞ strongly influence the form and position of the high-energy reflectivity minimum, especially at low temperatures, and the absolute value of reflectivity on the high-energy side. ϵ_∞ is therefore determined with a computational uncertainty of ± 0.5. Parameter Γ is quite sensitive to the plasmon edge. Therefore, at low temperatures (8, 30, and 58 °K) where this edge is not observed, no values for Γ can be given. Even at higher temperatures, the uncertainty on Γ is large (several cm^{-1}) and is given by the error bars of Fig. 19. In this same figure are given, for comparison, the values (black triangles) of the static damping constant γ, taken from Hall mobilities[13]:

$$\gamma(\mathrm{cm}^{-1}) = e/m_c \mu c \,, \tag{16}$$

where μ is the static mobility and c is the velocity of light. In the reflectivity fit, at low temperatures, the computed reflectivity is somewhat higher than the observed data near the lattice LO phonon frequency (reflectivity minimum).

V. PLASMON-PHONON COUPLING

In a simple model with one LO and one TO frequency, one expects two singularities[11,12] as two maxima of the function Im $-\epsilon^{-1}$ representing longitudinal modes. The frequencies generally labeled Ω_+ and Ω_- correspond to longitudinal oscillations with the lattice and electron plasma vibrating, respectively, in phase and 180° out of phase.[14]

In HgTe, the situation is more complex. Because of its band structure, the contribution $\Delta\epsilon'_{\mathrm{inter}}(\omega)$ must be included. Moreover, it is necessary to include another oscillator Ω_2 with strong polar character. This is shown in Fig. 20, where we have plotted as dots the square of the wave numbers of the maxima in $[\epsilon''/(\epsilon''^2+\epsilon'^2)](\mathrm{Im}-\epsilon^{-1})$ vs carrier concentration in units of $Ne^2/\pi c^2 m_c$. Arrows indicate the temperature corresponding to experimental data. These points correspond to longitudinal solutions. Stars indicate experimental maxima of ϵ''. Lines are the computed values of the maxima of ϵ'' and Im $-\epsilon^{-1}$ taken from Eqs. (11) and (12) with the parameters given in Figs. 15–19 and $F_1 = 4.7$. The existence of three longitudinal solutions is evident on curves of ϵ' computed by a Kramers-Krönig inversion (Fig. 14).

VI. DISCUSSION

With the experimental results that have been exhibited, and their interpretation, we could explain the features of the infrared spectrum of HgTe. Some points in our interpretation and the hypotheses used in the calculation have to be discussed. In this section we shall review the principal results on the phonon modes, discuss the influence of interband dielectric function values, examine the possible breakdown of the adiabatic approximation, and finally suggest some likely explanations for the origin of the Ω_2 mode.

In our measurements, as well as in those from other authors,[1] no satisfactory fit of reflectivity curves is possible if one does not take into account the contribution $\Delta\epsilon_{\mathrm{inter}}$ at all temperatures, but, especially at low temperatures, where $\Delta\epsilon_{\mathrm{inter}}$ has strong variation in the reststrahlen region. Results on reflectivity[2] at 80 °K were interpreted using the formulas of Sherrington and Kohn.[7] This interpretation is somewhat inaccurate since Eq. (4) in Ref. 2 contains an error coming from Sherrington and Kohn overlooking a factor of π in Eq. (15) of Ref. 13. Also, as was shown, $\Delta\epsilon_{\mathrm{inter}}$ varies significantly in the wavelength region between 8 and 80 °K. Our values for ω_{TO} and ω_{LO} at 8 °K are $\omega_{\mathrm{TO}} = 117$ cm^{-1}, $\omega_{\mathrm{LO}} = 132$ cm^{-1}, and the value for ϵ_∞ can be taken as 10.4 ± 0.5 at low temperatures. Our value for ω_{LO}, which is at the maximum of Im $-\epsilon^{-1}$, is significantly lower than that of Mooradian and Harman.[10] It is possible that in their case, this is due either to their being more than $\simeq 10^{16}$ cm^{-3} charge carriers or to heating the sample above at least 30 °K. Then, plasmon-phonon coupling can occur. In the zinc-blende structure of HgTe the effective charge is given by

$$\left(\frac{e^*}{e}\right)^2 = F_1 \Omega_1^2 \frac{9\pi}{4} \frac{a^3 M c^2}{(\epsilon_\infty + 2)^2 e^2} \,, \tag{17}$$

where a (lattice constant) is equal to 6.46×10^{-8} cm, and M is the reduced mass of ions. Equation (17) then gives a value of $e^*/e = 0.6$ at 8 °K, which is in

agreement with other determinations.[1]

Taking into account the contribution of $\Delta\epsilon_{\text{inter}}$ strongly modifies the values of the parameters, as had been pointed out in other optical studies by several authors.[2,15] In our case, a low-frequency fit of reflectivity is impossible, especially at low temperature, without this contribution. Other consequences are brought about by taking into account $\Delta\epsilon_{\text{inter}}(\omega)$ in the analysis of the results. In the low-energy region the contribution of $\Delta\epsilon_{\text{inter}}$ is the dominant contribution in the determination of the frequencies of the Ω_- mode. On the high-energy side, especially in the case of high temperatures or strongly doped crystals, $\Delta\epsilon'_{\text{inter}}$ is almost flat and of the same order of magnitude as ϵ_∞ (e.g., $\Delta\epsilon'_{\text{inter}} = 7$, $\epsilon_\infty = 7$ at 400 cm^{-1} and 300 °K) and the total $\Delta\epsilon'_{\text{inter}} + \epsilon_\infty = 14$. It would be a mistake to use this value as a "phenomenological" ϵ_∞ for the application of Drude-Zener theory to free-carrier absorption because, at this temperature and wave number $\Delta\epsilon''_{\text{inter}}$ is still about 2. Direct use of the Drude-Zener theory under these conditions would, for instance, lead for this reason to erroneous values of m_c^* calculated by this method.

With the form for $\Delta\epsilon_{\text{inter}}$, on the contrary, this fit can always be done within the limits of experimental error, with the notable exception of the Ω_+ reflectivity minimum, where a better fit would imply modifying the value of $\Delta\epsilon_{\text{inter}}$ in this region. One is aware, at the start, that the way we wrote the value of $\epsilon(\omega)$, in Eq. (1), implies that the adiabatic approximation is valid and that all oscillators are independent. This clearly must not be the case, especially when the interband transitions have a value close to the LO phonon in the material. Among other things, a breakdown of the adiabatic approximation would be equivalent to modifying the wave functions of electrons and therefore the matrix elements, especially for $\hbar\omega_F < \hbar\omega_{\text{LO}}$. At the present time, no complete theory has, to our knowledge, been published, although work is in progress on this point.[16] For lack of other information, we therefore treated the problem as an adiabatic one, suggesting that the small discrepancy between experiment and best fit at the LO reflectivity minimum is due to a partial breakdown of this approximation.

An interesting problem is the origin of the Ω_2 oscillator. This oscillator is fairly strong ($F_2 > 1$) at high temperatures. It couples with the plasmon mode and gives an Ω_+ mode between Ω_2 and Ω_1 (TO). Its oscillator strength increases with temperature (Fig. 17). It becomes so weak at 8 °K that it becomes inobservable. Such a mode is present apparently in $Cd_{0.2}Hg_{0.8}Te$[17] although the authors of Ref. 17 do not draw attention to it. We do not plan here to give a definite explanation of its origin, but rather list some possibilities in order of increasing likeliness. It is difficult to assign this mode to some electronic process because of its temperature dependence and polarization character. For the same reason, and also its intensity, multiple phonon absorption is unlikely: either addition or difference processes would have different temperature dependence, whatever the frequencies used. Phonon excitation at the edge of the Brillouin zone can be induced by a high density of impurities and have been observed in nonpolar[18] and polar[19] crystals at points of high density of states. Those peaks are, as a rule, orders of magnitude smaller (a few cm^{-1}) and in the case of HgTe, they would imply an extremely large number of defects. Nevertheless, this explanation cannot be ruled out, despite the temperature variation of F_2.

A gap mode would be a more satisfactory explanation. A calculation based on a simple model[20] shows that the local mode of Te substituted to Hg falls outside the phonon frequency gap. Conversely, mercury substituted to tellurium would give a gap mode at 105 cm^{-1} (as compared to $\Omega_2 = 105$ cm^{-1} at low temperatures). Actually, this may be coincidental since apparently the density of defects is high enough for the wave function of the corresponding phonons to extend to neighboring defects sites. In this situation the wave can propagate and have transverse and longitudinal character. Therefore, these frequencies, calculated for local modes, must be taken only as approximations for a high density of defects.

It is possible to build up a model for electrically neutral mercury substitutionals with Hg in the so-called "monovalent state." The existence of a $(2\text{Hg})^{++}$ complex has long been known to exist and compounds like Hg_2S and Hg_2Se have been prepared.[21] Here, a high concentration of Hg in the $(2\text{Hg})^{++}$ valency state would be the kind of defect least likely to affect electrical properties, since it would amount to a solid solution of Hg_2Te in HgTe; this type of defect would arise by substituting Hg to Te into 3 (HgTe) pairs, thus giving 2 (Hg_2Te). Unfortunately, evidencing this hypothesis is not straightforward and we can only suggest it as a possibility.[22] Additional weight is given to this explanation by the fact that HgTe grown from stoichiometric melts is consistently p type. Indeed, creation of Hg_2Te defects in HgTe leaves extra tellurium as a p-type doping agent. Those defects would be then responsible for the Ω_2 mode which we also observed by reflectivity experiments in HgTe crystals grown from the melt by the method of Bridgman.

VII. CONCLUSION

Experimental determination of the dielectric constant in HgTe in the region 80–300 cm^{-1} has been compared with theory. Taking into account

the contribution of interband transitions close to the Γ_8 extrema, it was possible to study two discrete transverse oscillators, Ω_1 and Ω_2, and plasmon-phonon modes connected with those oscillators in the range 8–300 °K. The values of the fundamental LO and TO modes were given at low temperatures and it was shown that phonon-plasmon coupling at all temperatures can be quantitatively accounted for, with the parameter used in the reflectivity fit. We have discussed but, from the data we have at present, were unable to ascertain the origin of an extra mode, Ω_2. If indeed this mode is linked to the presence of a high concentration of defects, it would be in contradiction with other data on HgTe, which suggests the presence of a large number of lattice defects, even in the best crystals studied.

ACKNOWLEDGMENTS

We should like to thank Dr. A. Mycielski for providing HgTe samples and Dr. J. M. Besson and Dr. G. Martinez for stimulating discussions, critical remarks, and aid in drawing up this paper. One of us (M. G.) wants to thank Delegation Generale ala Recherche Scientifigue et Technique for their kind invitation and financial support of this work.

---

*On leave from the Institute of Experimental Physics, Warsaw University, Warsaw, Poland.

[1]D. H. Dickey and J. G. Mavroides, Solid State Commun. 2, 213 (1964).

[2]W. J. Ivanov-Omskii, B. T. Kolomeiets, A. A. Malkova, Iu. F. Markov, and A. Ch. Mehtiev, Fiz. Tverd. Tela 4, 264 (1970) [Sov. Phys.-Solid State 4, 352 (1970)].

[3]J. G. Broerman, Phys. Rev. B 1, 4568 (1970).

[4]L. Liu and D. Brust, Phys. Rev. Lett. 13, 651 (1968).

[5]J. G. Broerman, Phys. Rev. B 2, 1818 (1970).

[6]J. G. Broerman, Phys. Rev. 183, 754 (1969).

[7]D. Sherrington and W. Kohn, Phys. Rev. Lett. 21, 153 (1968).

[8]J. G. Broerman, Phys. Rev. B 7, 4625 (1973).

[9]R. Le Toullec, Ph. D. thesis (Paris, 1968) (unpublished).

[10]A. Mooradian and T. C. Herman, in *Proceedings of the Conference on the Physics of Semimetals and Narrow-Gap Semiconductors, Dallas*, 1970, edited by D. L. Carter and R. T. Bate (Pergamon, New York, 1970), p. 297.

[11]A. Mooradian and G. B. Wright, Phys. Rev. Lett. 16, 999 (1966); R. W. Stimets and B. Lax, Phys. Rev. B 1, 4720 (1970).

[12]B. B. Varga, Phys. Rev. 137, A1896 (1965).

[13]V. I. Ivanov-Omskii, B. T. Kolomiets, V. K. Ogorodnikov, and K. P. Smekalova, Fiz. Tverd. Tela 4, 417 (1970) [Sov. Phys.-Solid State 4, 214 (1970)].

[14]E. Burstein, in *Elementary Excitations in Solids*, edited by A. A. Maradudin and G. F. Nardelli (Plenum, New York, 1969), p. 367.

[15]A. Mycielski, Ph. D. thesis (Warsaw, 1970) (unpublished); V. I. Ivanov-Omskii, B. T. Kolomiets, A. A. Malkova, Yu. F. Markov, A. Sh. Mekhtiev, and K. P. Smekalova, Fiz. Tverd. Tela 3, 1669 (1969) [Sov. Phys.-Solid State 3, 1403 (1970)].

[16]D. Sherrington, J. Phys. C 4, 2771 (1972).

[17]D. L. Carter, M. A. Kinch, and D. D. Buss, in Ref. 10, p. 273.

[18]M. Balkanski and W. Nazarewicz, J. Phys. Chem. Solids 23, 573 (1962).

[19]G. A. Slack and S. Roberts, Phys. Rev. B 3, 2613 (1971).

[20]S. P. Gaur, J. F. Vetelino, and S. S. Mitra, J. Phys. Chem. Solids (to be published).

[21]A number of references can be found on this point, for instance, in P. Pascal, *Nouveau Traité de Chimie Minérale*, edited by C. Masson (Da Capo, New York, 1962), Vol. 5.

[22]We are indebted to Dr. J. M. Besson for having suggested this mechanism.